DOI: 10.1002/cmdc.201500040

Can Silicon Make an Excellent Drug Even Better? An in vitro and in vivo Head-to-Head Comparison between Loperamide and Its Silicon Analogue Sila-Loperamide

Marcel Geyer,[a] Eric Wellner,[b] Ulrik Jurva,[b] Sebastian Saloman,[a] Duncan Armstrong,[c] and Reinhold Tacke*[a]

Loperamide (**1a**), an opioid receptor agonist, is in clinical use as an antidiarrheal agent. Carbon/silicon exchange (sila-substitution) at the 4-position of the piperidine ring of **1a** ($R_3COH \rightarrow R_3SiOH$) leads to sila-loperamide (**1b**). Sila-loperamide was synthesized in a multistep procedure, starting from triethoxyvinylsilane and taking advantage of the 4-methoxyphenyl (MOP) unit as a protecting group for silicon. The in vitro and in vivo pharmacokinetic (PK) and pharmacodynamic (PD) properties of the C/Si analogues **1a** and **1b** were determined and compared. Despite significant differences in the in vitro PK properties of loperamide and sila-loperamide regarding clearance, permeability, and efflux, both compounds exhibited nearly identical in vivo PK profiles. The increase in metabolic stability of the silicon compound **1b** observed in vitro seems to be counterbalanced by an increase in efflux and diminished permeability compared to the parent carbon compound **1a**. Overall, sila-loperamide exhibits high unbound clearance (CL_u), leading to a significant decrease in unbound concentration (C_u) and unbound area under the curve (AUC_u) after oral exposure, compared to loperamide. In vitro and in vivo metabolic studies showed an altered profile of biotransformation for the silicon compound **1b**, leading to the formation of a more polar and quickly cleared metabolite and preventing the formation of the silicon analogue of the neurotoxic metabolite observed for the parent carbon compound **1a**. These differences can be correlated with the different chemical properties of the C/Si analogues **1a** and **1b**. This study provides some of the most detailed insights into the effects of a carbon/silicon switch and how this carbon/silicon exchange affects overall drug properties.

Introduction

2,2-Diphenyl-4-(4-aryl-4-hydroxypiperidino)butyramides were developed as antidiarrheal agents in the early 1970s by Janssen and co-workers, and loperamide (**1a**) was selected for further clinical investigation.[1] Today, loperamide is the most sold over-the-counter antidiarrheal agent in the world, with a well-known metabolic fate.

In context with our systematic studies on silicon-based drugs,[2,3] we sought to examine the biological effects of sila-substitution (C/Si exchange) of the quaternary R_3COH carbon atom of the 4-(4-chlorophenyl)-4-hydroxypiperidino group of **1a**. The carbon/silicon switch strategy, i.e., the strategic replacement of a carbon atom with a silicon atom within a well-known drug, with the rest of the molecule remaining unaltered, is a well-established method for the design and development of new silicon-based drugs.[2,3] Incorporation of silicon into a drug can affect and, ideally, improve the pharmacodynamics (PD) and pharmacokinetics (PK).

Herein we report the synthesis of sila-loperamide (**1b**) and present a detailed comparison between the physicochemical properties and the primary in vitro PD and PK properties of the C/Si analogues **1a** and **1b**. We also report the profiling of primary safety aspects, such as CYP inhibition, time-dependent CYP inhibition, CYP reaction phenotyping (CRP), and hERG inhibition. We also present an assessment of the impact of the carbon/silicon switch on permeability, efflux, protein binding, and reactive metabolite formation. Most importantly, we report a head-to-head comparison of the in vivo PK and metabolic profiles of the C/Si analogues **1a** and **1b**. This allows unique insight into the behavior of a silicon-containing drug and the translation of its in vitro properties into an in vivo situation.

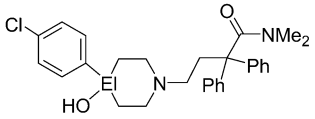

El = C: loperamide (**1a**)
El = Si: sila-loperamide (**1b**)

[a] M. Geyer, S. Saloman, Prof. Dr. R. Tacke
Universität Würzburg, Institut für Anorganische Chemie
Am Hubland, 97074 Würzburg (Germany)
E-mail: r.tacke@uni-wuerzburg.de

[b] Dr. E. Wellner, Dr. U. Jurva
AstraZeneca R&D Mölndal, CVMD Innovative Medicines
Pepparedsleden 1, 43183 Mölndal (Sweden)

[c] Dr. D. Armstrong
AstraZeneca, Drug Safety & Metabolism
Alderley Park, Mereside, SK10 4TG (UK)

Results and Discussion

Synthesis

Sila-loperamide (**1b**) was synthesized in a multistep procedure, starting from commercially available triethoxyvinylsilane (**2**) and taking advantage of the 4-methoxyphenyl (MOP) unit as a protecting group for silicon (Scheme 1). Thus, treatment of **2** with (4-chlorophenyl)magnesium bromide afforded (4-chlorophenyl)diethoxyvinylsilane (**3**), which upon sequential treatment with (4-methoxyphenyl)magnesium bromide and vinylmagnesium chloride gave (4-chlorophenyl)(4-methoxyphenyl)-divinylsilane (**4**). Reaction of **4** with 9-borabicyclo[3.3.1]nonane (9-BBN),[4] followed by sequential treatment with aqueous solutions of sodium hydroxide and hydrogen peroxide, yielded (4-chlorophenyl)bis(2-hydroxyethyl)(4-methoxyphenyl)silane (**5**). Reaction of **5** with methanesulfonyl chloride, in the presence of triethylamine, and subsequent treatment with a large excess of allylamine afforded 1-allyl-4-(4-chlorophenyl)-4-(4-methoxyphenyl)-4-silapiperidine (**6**). Reaction of **6** with 1-chloroethyl chloroformate,[5] followed by treatment with methanol, yielded 4-(4-chlorophenyl)-4-(4-methoxyphenyl)-4-silapiperidinium chloride (**7**·HCl). Compound **7**·HCl was then treated with dimethyl(tetrahydro-3,3-diphenyl-2-furylidene)ammonium bromide[6] (**8**) and sodium carbonate to give 4-(4-chlorophenyl)-1-(4-dimethylamino-4-oxo-3,3-diphenylbutyl)-4-(4-methoxyphenyl)-4-silapiperidine (**9**). Treatment of **9** with trifluoromethanesulfonic acid, followed by reaction with triethylammonium chloride (cleavage of the 4-methoxyphenyl protecting group to give the corresponding chlorosilane) and subsequent treatment with methanol and triethylamine, gave 4-(4-chlorophenyl)-1-(4-dimethylamino-4-oxo-3,3-diphenylbutyl)-4-methoxy-4-silapiperidine (**10**) as an intermediate (not further purified; identified by high-resolution mass spectrometry), which, upon hydrolysis, finally afforded the target compound 4-(4-chlorophenyl)-1-(4-dimethylamino-4-oxo-3,3-diphenylbutyl)-4-hydroxy-4-silapiperidine (sila-loperamide, **1b**).

Compounds **3**, **4**, and **6** were isolated as colorless liquids, whereas **1b**, **5**, **7**·HCl, and **9** were obtained as colorless solids. The identities of all these compounds were established by elemental analyses (**3**, **4**, **5**, **6**, **7**·HCl) or high-resolution mass spectrometry (**1b**, **9**) and by NMR spectroscopic studies (^{1}H, ^{13}C, and ^{29}Si).

Physicochemical properties

Loperamide (**1a**) and sila-loperamide (**1b**) were studied for their octanol/water (pH 7.4) distribution coefficient (log *D* value), dissociation constant in water (pK_a value), and solubility in HBSS buffer (pH 7.4). As can be seen from Table 1, the re-

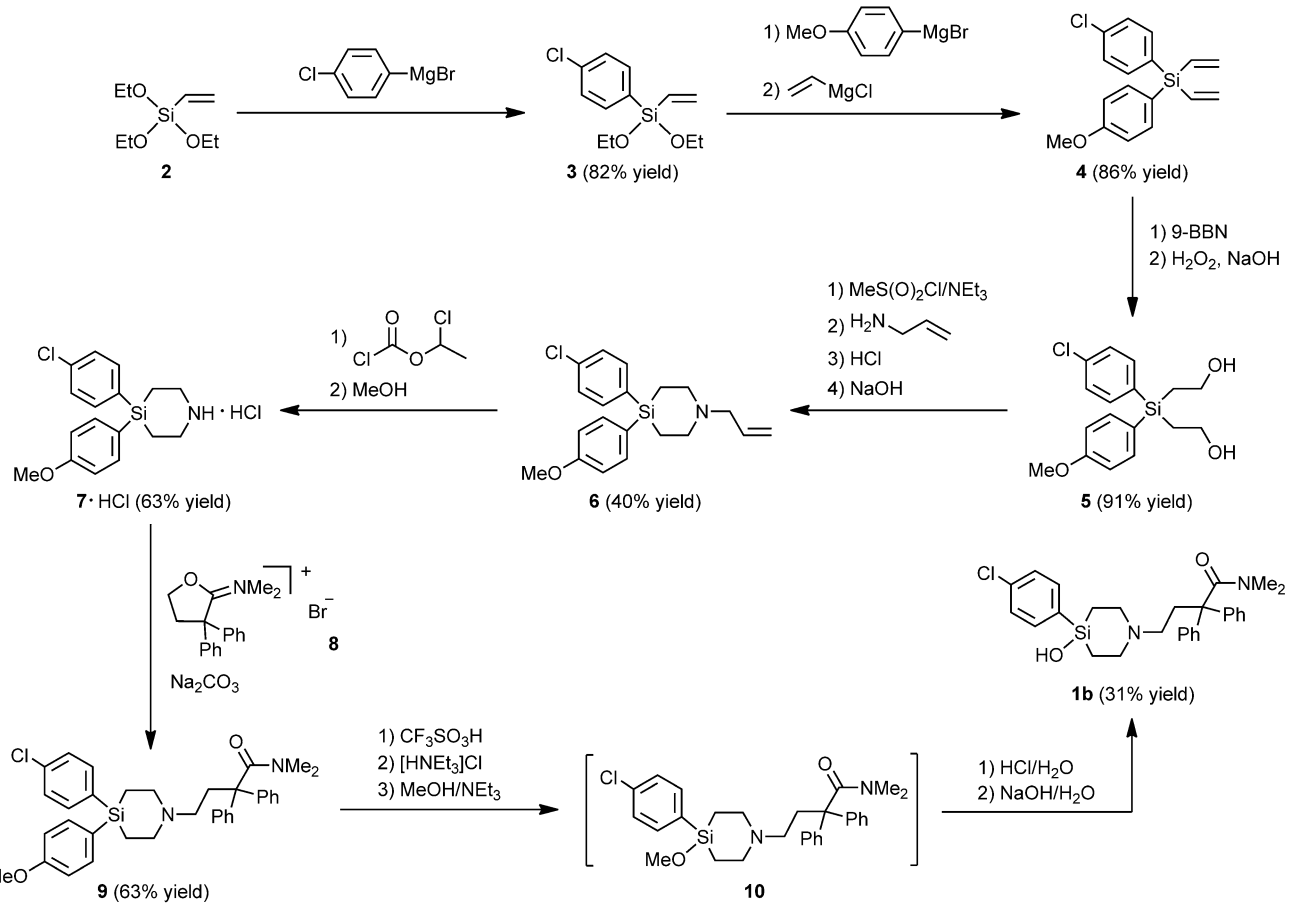

Scheme 1. Synthesis of sila-loperamide (**1b**).

Table 1. Physicochemical properties of **1a** and **1b**.

Compd	log D[a]	pK_a[b]	Solubility [μM][c]
1a	3.53 ± 0.03	9.12 ± 0.11	19 ± 3
1b	3.73 ± 0.07	8.93 ± 0.26	30 ± 9

[a] Determined at pH 7.4; values represent the mean ± SEM (n = 3). [b] Values represent the mean ± SEM (**1a**: n = 3; **1b**: n = 4). [c] Determined in HBSS buffer (pH 7.4); values represent the mean ± SEM (**1a**: n = 3; **1b**: n = 5).

spective data for the C/Si analogues **1a** and **1b** are each within the same range, indicating that the carbon/silicon switch has no major impact on the physicochemical properties. Both compounds are protonated at ~97% at pH 7.4, as shown by their pK_a values.

In vitro pharmacology

The binding affinities and functional effects of loperamide (**1a**) and sila-loperamide (**1b**) at the human μ1 opioid receptor and rat κ1 opioid receptor were investigated. Binding affinities and agonistic potencies are listed in Table 2. Loperamide is reported to have a K_i value of 3.3 nM for the human μ opioid receptor.[7] In our μ1 opioid receptor affinity binding assay, loperamide was much more potent (K_i = 0.12 nM). Sila-loperamide was found to be fourfold less potent (K_i = 0.53 nM) than loperamide. The competition binding and functional dose–response curves of compounds **1a** and **1b** for the human μ1 opioid receptor are shown in Figure 1. Both **1a** and **1b** were found to be full agonists at the μ1 opioid receptor, as can be seen from Figure 1 A. However, the potency shift in this functional assay was more pronounced for sila-loperamide (EC_{50} = 1.1 nM), whereas the potency of the parent carbon compound loperamide was in the low picomolar range (EC_{50} = 60 pM). The potency increase in the efficacy assay might result from overexpression of the receptor in CHO cells, resulting in a large receptor reserve.[8] In context with our assay, the decreased potency of **1b** indicates that the silicon analogue is less effective in activating the receptor than the parent carbon compound **1a**.

Table 2. Binding affinity (pK_i) and agonistic potency (pEC_{50}) of **1a** and **1b** at the human μ1 opioid receptor (μ1OPR) and rat κ1 opioid receptor (κ1OPR).

Compd	μ1OPR[a,b]		κ1OPR[a,c]	
	pK_i	pEC_{50}	pK_i	pEC_{50}
1a	9.91 ± 0.17 (0.12 nM)	10.19 ± 0.15 (0.06 nM)	7.19 ± 0.09 (65 nM)	7.46 ± 0.26 (35 nM)
1b	9.27 ± 0.09 (0.53 nM)	8.96 ± 0.32 (1.1 nM)	6.44 ± 0.06 (364 nM)	6.29 ± 0.23 (517 nM)

[a] Molar values are given in parentheses. [b] Values represent the mean ± SD (n = 3). [c] Values represent the mean ± SD (n = 4).

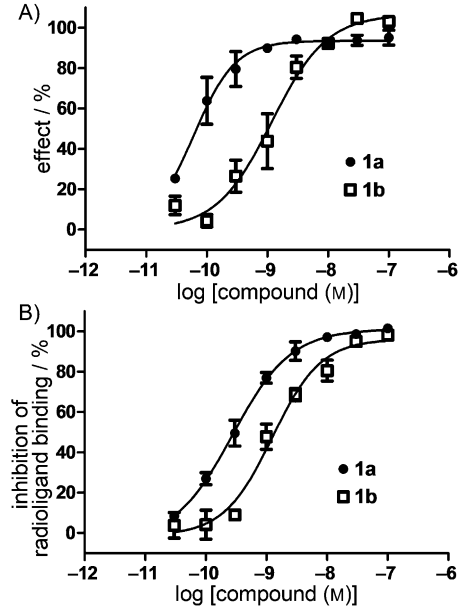

Figure 1. A) Dose–response curves of **1a** and **1b** at the human μ1 opioid receptor in a cell-based functional assay. B) Competition binding curves of compounds **1a** and **1b** at the human μ1 opioid receptor. The stronger left shift of the curve of **1a** relative to that of **1b** in the agonistic efficacy assay might result from a more effective engagement of the receptor reserve by loperamide than by sila-loperamide.

Affinity and functional potency of **1a** and **1b** at the rat κ1 opioid receptor show a trend similar to that observed for the human μ1 opioid receptor system studied.

hERG activity

The inhibitory effect of loperamide (**1a**) and sila-loperamide (**1b**) at the hERG potassium ion channel was tested to assess the risk of QT interval prolongation.[9] Loperamide showed no inhibitory effect at the test concentration of 11 μM in the hERG spot test. In the same spot test, sila-loperamide had an inhibitory effect of 83%, and therefore the IC_{50} of **1b** was determined. The silicon compound **1b** blocked the potassium channel with a mean IC_{50} value of 3.64 μM. This is ~6700-fold higher than the EC_{50} value of **1b** at the human μ1 opioid receptor.

Apparent permeability in human Caco-2 and MDCK-MDR1 cells

Loperamide (**1a**) is a peripherally acting drug,[10] and in vitro and in vivo studies have shown that it is subject to P-glycoprotein (P-gp)-mediated efflux. The poor permeability and efflux might limit the uptake of loperamide,[11] resulting in low oral bioavailability.

To obtain information about their apparent permeability (P_{app}), loperamide (**1a**) and sila-loperamide (**1b**) were studied in a human Caco-2 cell model (Table 3). For the apical-to-basolateral (A→B) transport, the apparent permeability was moderate for **1a** ($P_{app} = 2.57 \times 10^{-6}$ cm s^{-1}) and low for **1b** (P_{app} = 0.63 ×

Table 3. Apparent permeability (P_{app}) and efflux ratio (ER) of **1a** and **1b** in human Caco-2 and MDCK-MDR1 cells.

Compd	Cells	P_{app} [10^{-6} cm s^{-1}] A→B	B→A	ER	Recovery [%][c]
1a	Caco-2[a]	2.57 ± 0.08	13.8 ± 0.38	5	50 < x < 66
1b	Caco-2[a]	0.63 ± 0.02	7.72 ± 0.44	12	30 < x < 47
1a	MDCK-MDR1[b]	0.89	11.2	13	40 < x < 66
1b	MDCK-MDR1[b]	0.34	5.57	34	20 < x < 38

[a] Values represent the mean ± SD (n = 3). [b] Values represent the mean (n = 2). [c] Values represent the range for the A→B and B→A recovery.

10^{-6} cm s^{-1}). The efflux ratio ([P_{app} A→B]/[P_{app} B→A]) was high for both compounds (ratio: 5 for **1a** and 12 for **1b**). Results from the MDCK-MDR1 cell line confirmed that both compounds are substrates for P-gp-mediated efflux (ratio: 13 for **1a** and 34 for **1b**). The A→B permeability in this cell line was low for both compounds. Overall, these data suggest that the oral bioavailability of loperamide and sila-loperamide might be limited due to their 1) low permeability and 2) high efflux ratio.[12] The Caco-2 data indicate an even more pronounced permeability limitation for the silicon compound **1b**, which could translate into improved safety margins for sila-loperamide and decreased partition into the central nervous system (CNS). The recovery in Caco-2 and MDCK-MDR1 cells for both A→B and B→A transport is generally low, indicating metabolism of **1a** and **1b** within these cells or adsorption of the compounds. Regarding the moderate intrinsic clearance of **1a** and **1b** in human hepatocytes (see below), adsorption of the compounds at the surface is the more probable cause for the low recovery rate.

Intrinsic clearance and half-life in human and rat hepatocytes and human liver microsomes

The clearance rates of loperamide (**1a**) and sila-loperamide (**1b**) were measured in human liver microsomes (Table 4). Although the microsome fractions contain many drug-metabolizing enzymes such as cytochrome P450s (CYPs), flavin monooxygenases, carboxylesterases, and epoxide hydrolases, they do not allow assessment of the possibility of phase II biotransformation. Therefore, to assess the potential impact of phase II metabolism, we also measured the metabolic stability of the C/Si analogues **1a** and **1b** in human and rat hepatocytes (Table 4). The intrinsic clearance (CL_{int}) was determined to be medium in human liver microsomes (44.3 μL min^{-1} mg^{-1} for **1a** and 46.9 μL min^{-1} mg^{-1} for **1b**) and medium to high in human hepatocytes (13.1 μL min^{-1} mg^{-1} for **1a** and 8.60 μL min^{-1} mg^{-1} for **1b**), indicating that the uptake into hepatocytes was not limited by the medium-to-poor permeability and strong efflux of the compounds. The intrinsic clearance in rat hepatocytes was significantly higher, resulting in a substantial shortening ($\Delta t_{1/2} = t_{1/2hu} - t_{1/2rat}$) of the half-life ($\Delta t_{1/2}$ = 46.7 min for **1a** and $\Delta t_{1/2}$ = 70.2 min for **1b**).

CYP inhibition, time-dependent CYP inhibition, and CYP reaction phenotyping

Loperamide (**1a**) and sila-loperamide (**1b**) are weak-to-medium inhibitors of several CYP isoforms. The results of our studies of CYP inhibition are summarized in Table 5. Both CYP2D6 (**1a**, IC_{50} = 0.9 μM; **1b**, IC_{50} = 0.8 μM) and CYP3A4 (**1a**, IC_{50} = 1.7 μM; **1b**, IC_{50} = 1.0 μM) exhibit the strongest inhibition by **1a** and **1b**. No time-dependent inhibition of any isoform was observed for either compound. This means that neither **1a** nor **1b** form metabolites, which are capable of significantly inhibiting any of the CYPs investigated.

Table 5. Cytochrome P450 inhibition (IC_{50}) by **1a** and **1b**.

Compd	IC_{50} [μM][a] CYP3A4	CYP2C9	CYP1A2	CYP2C19	CYP2D6	CYP2C8
1a	1.7 ± 0.5	11 ± 0.5	> 20	11 ± 0.2	0.9 ± 0.1	> 20
1b	1.0 ± 0.1	9.6 ± 1.1	> 20	4.8 ± 0.7	0.8 ± 0.1	> 20

[a] Values represent the mean ± SD (n = 3).

CYP reaction phenotyping (CRP) is a tool to investigate the contribution of various CYPs to total metabolic clearance. This information can be used to evaluate the risk of drug–drug interactions. According to Kim et al.,[13] loperamide is metabolized mainly by CYP3A4 and CYP2C8. Figure 2 summarizes our results of CRP. It has been shown that while CYP3A4 is the predominant hepatic form of CYP3A, in many cases CYP3A5 contributes significantly to the total liver clearance.[14] Therefore, CYP3A5 was included in the CRP panel to provide a more differentiated view on total CYP3A contribution relative to published work thus far. Both loperamide and sila-loperamide are metabolized by CYP3A4 to > 95%. CYP3A5 contributes by ~1% to CYP oxidation, followed by CYP2C8. Sila-loperamide displays a nearly identical CRP profile to that of the parent carbon compound **1a**. It offers no major alternative oxidation pathway to escape the extensive CYP3A4 metabolism.

Table 4. Intrinsic clearance (CL_{int}) and half-life ($t_{1/2}$) of **1a** and **1b** in human/rat hepatocytes and human liver microsomes.

Compd	hu hep CL_{int} [μL min^{-1} mg^{-1}]	hu hep $t_{1/2}$ [min]	rat hep CL_{int} [μL min^{-1} mg^{-1}]	rat hep $t_{1/2}$ [min]	hu liv mic CL_{int} [μL min^{-1} mg^{-1}]	hu liv mic $t_{1/2}$ [min]
1a	13.07 ± 1.13[a]	54.28 ± 4.72[a]	91.57 ± 5.71[c]	7.60 ± 0.47[c]	44.27 ± 9.46[c]	15.53 ± 3.16[c]
1b	8.60 ± 0.52[b]	82.19 ± 5.28[b]	58.51 ± 4.50[c]	11.99 ± 0.90[c]	46.90 ± 0.47[c]	14.78 ± 0.15[c]

[a] Values represent the mean ± SD (n = 4). [b] Values represent the mean ± SD (n = 6). [c] Values represent the mean ± SD (n = 3).

Rat in vivo PK and plasma protein binding

Rat in vivo PK data for loperamide (**1a**) was reported in 2012.[11] Table 6 sum-

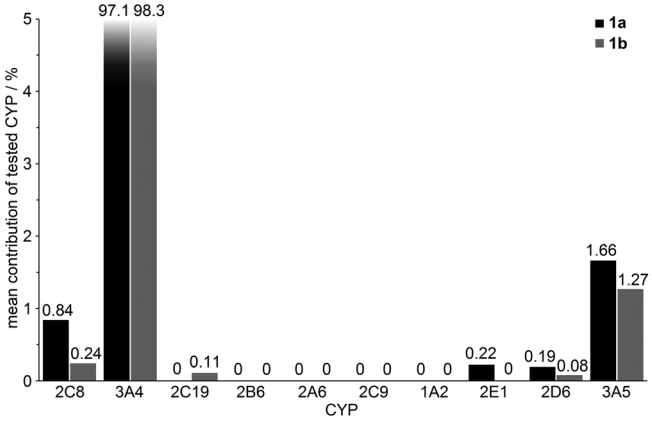

Figure 2. CRP of compounds **1a** and **1b**. Both compounds are mainly metabolized by CYP3A4 and CYP3A5. While the silicon compound **1b** is a weak substrate for CYP2C19, it is more selective against CYP2E1 and CYP2D6 than the parent carbon compound **1a**.

Table 6. In vivo PK data of **1a** in Sprague–Dawley rats and **1a** and **1b** in Han Wistar rats.

Parameter	**1a**[a]	**1a**[b]	**1b**[b]
i.v. dosing			
CL [mL min^{-1} kg^{-1}]	128[c]	30[d]	27[d]
CL_u [mL min^{-1} kg^{-1}]	2667[c]	517[d]	1800[d]
V_{SS} [L kg^{-1}]	9[c]	4[d]	4[d]
$t_{1/2}$ [h]	1[c]	2[d]	3[d]
fu_{rat} [%]	4.8	5.8	1.5
fu_{hu} [%]	8.1	8.1	2.8
p.o. dosing			
F [%]	43[c]	4[d]	8[d]
$t_{1/2}$ [h]	13[c]	11.5[d]	15[d]
C_{max} [μM]	0.19[c]	0.02[d]	0.04[d]
$C_{u,max}$ [nM]	9[c]	1.2[d]	0.6[d]
AUC [μmol h^{-1}]	1.69[c]	0.39[d]	0.72[d]
AUC_u [μmol h^{-1}]	0.08	0.02	0.01

[a] Sprague–Dawley; results taken from reference [11]. [b] Han Wistar; values represent the mean ($n=2$). [c] Dose: 5.5 μmol kg^{-1} i.v. or 21 μmol kg^{-1} p.o. [d] Dose: 5.1 μmol kg^{-1} i.v. or 10.1 μmol kg^{-1} p.o.

marizes the published PK data for **1a** in male Sprague–Dawley rats and our own data for **1a** and its silicon analogue sila-loperamide (**1b**) in male Han Wistar rats. Differences observed between published data and our in-house data might result from differences in dosing or more likely from the use of different rat strains.

In our hands, loperamide has an oral bioavailability (F) of 4% and a clearance (CL) of 30 mL min^{-1} kg^{-1} (dose: 5.1 μmol kg^{-1} i.v.).[15] The rat plasma binding (fu_{rat}) of **1a** was determined in Han Wistar rat plasma to be 5.8%, with a recovery rate of 95%, indicating the high stability of loperamide in rat plasma. The total plasma concentration (C_{max}) after oral administration (dose: 10.1 μmol kg^{-1} p.o.) is 0.02 μM, resulting in total plasma concentration unbound ($C_{u,max}$) of 1.2 nM. The volume of distribution (V_{ss}) is high (4 L kg^{-1}), indicating a broad distribution into tissue. The half-life ($t_{1/2}$) of **1a** is 2 h (dose: 5.1 μmol kg^{-1} i.v.). For an oral dose of 10.1 μmol kg^{-1}, the observed half-life was much higher ($t_{1/2}=11.5$ h). Delayed dissolution, continuous absorption, decrease in gut motility, and the enterohepatic recirculation of **1a**[16,17] are possible explanations for the prolongation of the half-life after oral dosing.

The C/Si analogues **1a** and **1b** have a similar solubility and lipophilicity. Furthermore, both compounds are strong P-gp substrates, having medium-to-poor permeability. The strong efflux observed for **1a** and **1b** in Caco-2 and MDCK-MDR1 cells, combined with their limited permeability and low solubility, seems to substantially restrict their oral bioavailability and systemic exposure in our models.

After i.v. and p.o. administration, sila-loperamide exhibits an in vivo PK profile nearly identical to that of the parent carbon compound loperamide. Parameters such as CL, V_{SS}, and $t_{1/2}$ are in the same range for both compounds. Differences can be observed in oral bioavailability, which is 8% for sila-loperamide, and total concentrations in plasma ($C_{max}=0.04$ μM). Considering the lower unbound fraction of the silicon compound **1b** in the plasma, the unbound clearance (CL_u)[18] of **1b** is ~3.5-fold higher than that of its parent carbon compound **1a**. The high CL_u value leads to a significant drop in the $C_{u,max}$ value of **1b** (0.6 nM) relative to **1a** (1.2 nM).[19] Ultimately, this results in a lower area under the curve unbound (AUC_u; **1b**, 0.01 μmol h^{-1}; **1a**, 0.02 μmol h^{-1}) for **1b** despite the slight increase in oral bioavailability. It is well understood that P-gp-mediated secretion of a compound into the intestine and low permeability can have a profound impact by increasing the in vivo blood clearance (CL). In such cases, CL is often underpredicted by the in vitro intrinsic clearance (CL_{int}).[20] For lack of *Mdr1a* knockout rats, we tried to assess the qualitative impact of transporters and permeability on the in vivo clearance of **1a** and **1b** by comparing it with the predicted clearance of the compounds. Applying the well-stirred model,[21] the in vitro CL_{int} of **1b** in hepatocytes results in a predicted blood clearance CL_H[22] of 50 mL min^{-1} kg^{-1} and reflects the observed in vivo blood clearance ($CL=30$ mL min^{-1} kg^{-1}) surprisingly well, despite the high efflux ratio and low permeability[20] of **1b**. The intrinsic clearance of the parent carbon compound **1a** observed in rat hepatocytes leads to an overprediction of the in vivo clearance ($CL=30$ mL min^{-1} kg^{-1}) versus predicted blood clearance ($CL_H=52$ mL min^{-1} kg^{-1}). Overall, the blood clearance of the C/Si analogues **1a** and **1b** is predicted well by their intrinsic in vitro hepatocyte clearance, indicating that efflux and low permeability do not particularly impact the blood clearance, or are counterbalanced by other mechanisms such as redistribution from other compartments.

Considering that the motility effect of loperamide is mainly achieved via the opioid receptor in the gut, the lower $C_{u,max}$ and AUC_u values of sila-loperamide could improve safety margins, particularly with regard to side effects mediated by the opioid receptors in the brain.[23] Figure 3 shows the ratio of C_u after oral dosing and the EC_{50} values reported in Table 2, and it represents the free exposure above the EC_{50} value. While the free exposure of **1a** at the human μ1 opioid receptor is ~27-fold above the EC_{50} value, the low potency at the rat κ1 opioid

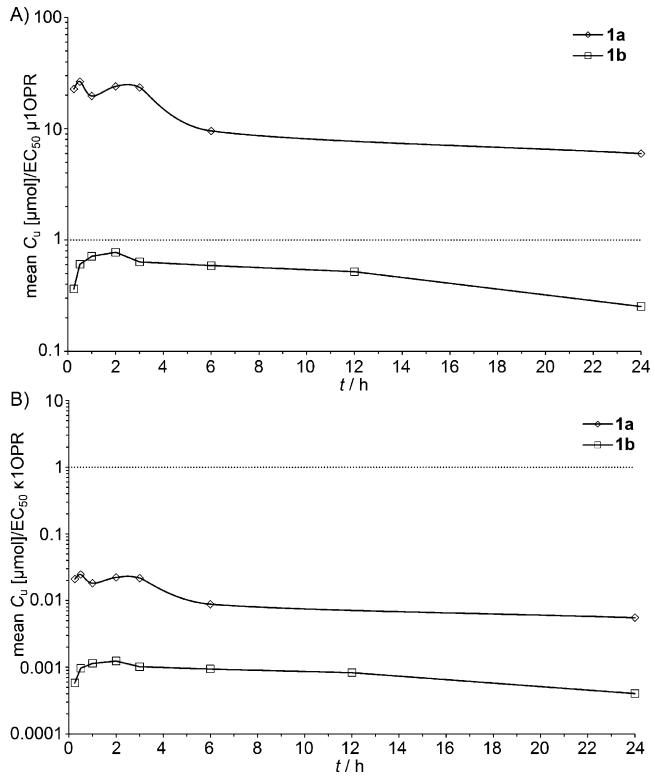

Figure 3. Ratio between measured free plasma concentration C_u and agonist EC_{50}, plotted against time, for compounds **1a** and **1b**. A) -Fold exposure of **1a** and **1b** at the human μ1 opioid receptor. B) -Fold exposure of **1a** and **1b** at the rat κ1 opioid receptor. Both compounds were orally administered at 12.2 μmol kg^{-1}. The horizontal dotted lines represent $C_u/EC_{50} = 1$ in each case and indicate the limit for free exposure above or below the measured agonist EC_{50} value. The two concentration maxima observed in the concentration versus time curves of **1a** might indicate enterohepatic recirculation.

receptor leads to no free exposure of the compound above its EC_{50} value. The free concentrations of the silicon analogue **1b** are just about to reach the EC_{50} value at the μ1 opioid receptor, but are almost 1000-fold below the EC_{50} value at the κ1 opioid receptor. Therefore, these data suggest that sila-loperamide provides a decrease in the free drug exposure after oral administration in rats, possibly leading to improved safety margins. In combination with the high efflux ratio and low permeability observed in Caco-2 and MDCK-MDR1 cells, the exposure of **1b** into the CNS might be even further decreased.

Identification of major in vitro metabolites and reactive metabolites

Two major metabolites of loperamide (**1a**), **M1a** and **M2a**, were identified in human hepatocytes (Table 7, Scheme 2). Similar observations were made in human liver microsomes.[24] Interestingly, we did not observe any formation of conjugates in the hepatocytes, which means that the aforementioned CYP3A4 metabolism seems to be the predominant route of biotransformation for both **1a** and **1b**. Considering the metabolic fate of haloperidol,[3c,25,26] which is metabolized into the potentially neurotoxic pyridinium cation HPP^+, we were interested in the formation of the possible neurotoxic LPP^+ metabolite **M4a** (Scheme 3).[24] After 40 min incubation of **1a** in human hepatocytes, **M4a** was observed to a minor extent (0.6%). In addition, the minor loperamide metabolites **M3a** and **M5a** were detected. The main metabolites of sila-loperamide (**1b**) in human hepatocytes are **M1b** and **M2b**, the silicon analogues of the main loperamide metabolites **M1a** and **M2a** (Table 8, Scheme 2). Further, α-oxidation (relative to the nitrogen atom) at the silapiperidine ring, followed by ring-opening

Table 7. Loperamide (**1a**) metabolites after an incubation period of 40 min in human hepatocytes.

Metabolite	t_R [min]	*m/z* Values (HRMS) Protonated parent species	Major MS–MS ions	Estimated formation [%]
1a	3.25	477.2303	477.2319, 266.1568, 238.1238, 210.1290	64
M1a	2.87	493.2256	493.2265, 463.2140, 282.1490, 252.1384, 196.1123	23
M2a	3.02	463.2142	463.2149, 252.1391, 224.1088, 196.1124	13
M3a	2.68	479.2107	479.2117, 449.1976, 268.1331, 238.1226, 182.0975	0.6
M4a	3.61	455.1847	455.1829, 430.4557, 297.0898, 266.0975	0.6
M5a	3.07	491.2101	450.1807, 280.1351, 252.1382, 224.0900, 196.1107	<0.1

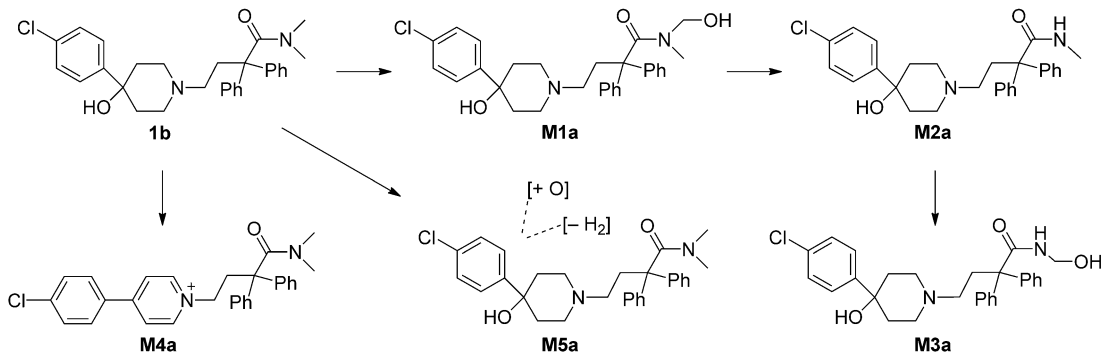

Scheme 2. Proposed metabolic pathways of loperamide (**1a**) in human hepatocytes. The structures of the proposed metabolites **M1a**, **M2a**, **M3a**, **M4a**, and **M5a** are tentative assignments based on accurate mass measurements and interpretation of MS–MS spectra.

Table 8. Sila-loperamide (**1b**) metabolites after an incubation period of 40 min in human hepatocytes.

Metabolite	t_R [min]	*m/z* Values (HRMS) Protonated parent species	Major MS–MS ions	Estimated formation [%]
1b	3.42	493.2076	493.2069, 266.1555, 238.1233, 210.1284	78
M1b	3.03	509.2021	509.2010, 479.1899, 282.1499, 252.1390, 196.1126	12
M2b	3.19	479.1907	479.1925, 252.1388, 196.1126	3
M3b	2.86	495.1862	495.1855, 465.1765, 420.1179, 268.1347, 238.1233	0.3
M4b	3.11	483.1855	483.1845, 420.1191, 266.1543, 238.1238, 210.1282	5
M5b	3.25	507.1861	507.1884, 466.1593, 420.1189, 252.1394, 196.1118	1

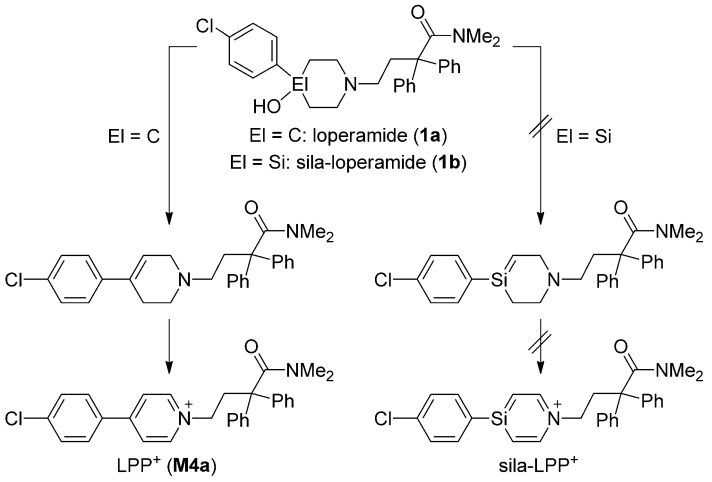

Scheme 3. Metabolism of loperamide (**1a**). Left: formation of the neurotoxic pyridinium metabolite LPP^+ (**M4a**).[24] Right: formation of sila-LPP^+ from sila-loperamide (**1b**) is not possible owing to chemical reasons (unstable Si=C double bond).

reaction, leads to the formation of a third major metabolite, the silanediol **M4b**. This result suggests that sila-loperamide has access to an alternative metabolic pathway leading to a more polar metabolite than loperamide itself. In addition, the two minor sila-loperamide metabolites **M3b** and **M5b** (the silicon analogues of the loperamide metabolites **M3a** and **M5a**) were detected. Because it is well understood that silapiperidine analogues cannot undergo a bioactivation to a silapyridinium cation,[3e] the generation of sila-LPP^+ is not expected.

Human microsome metabolite trapping reactions to identify glutathione conjugates and nitrile or methoxyamine adducts of **1a** and **1b** were all negative and did not reveal the formation of any reactive metabolites.

Identification of major metabolites in vivo in plasma from male Han Wistar rats

The plasma samples from the in vivo PK experiments (see *Rat in vivo PK and plasma protein binding* section above) were analyzed with respect to metabolites as well as parent drug to allow the generation of metabolic profiles. The relation between loperamide (**1a**) and sila-loperamide (**1b**) and their metabolites identified in rat plasma following i.v. administration of **1a** (dose: 5.5 $\mu mol\,kg^{-1}$) and **1b** (dose: 5.1 $\mu mol\,kg^{-1}$) is shown in Figure 4. For both compounds, the two major metabolites **M1a**/**M1b** and **M2a**/**M2b** from the in vitro metabolite identification experiments (Tables 7 and 8, Schemes 2 and 4) were also identified as major circulating metabolites in vivo. The origin of these metabolites is hydroxylation on the dimethylamino moiety, and clearly, this is a favored metabolic pathway for both **1a** and **1b** in vitro as well as in vivo. Metabolites **M2a**/**M2b** are formed chemically from **M1a**/**M1b**, and it should be noted that the difference in levels between **M1a** and **M1b** could originate from small differences in sample handling. The metabolites **M1a**/**M1b** and **M2a**/**M2b** were relatively stable in the circulation. Inspection

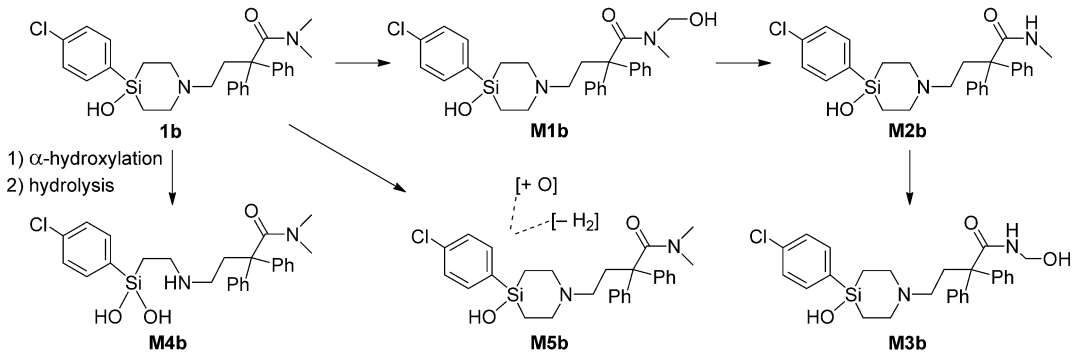

Scheme 4. Proposed metabolic pathways of sila-loperamide (**1b**) in human hepatocytes. The structures of the proposed metabolites **M1b**, **M2b**, **M3b**, **M4b**, and **M5b** are tentative assignments based on accurate mass measurements and interpretation of MS–MS spectra.

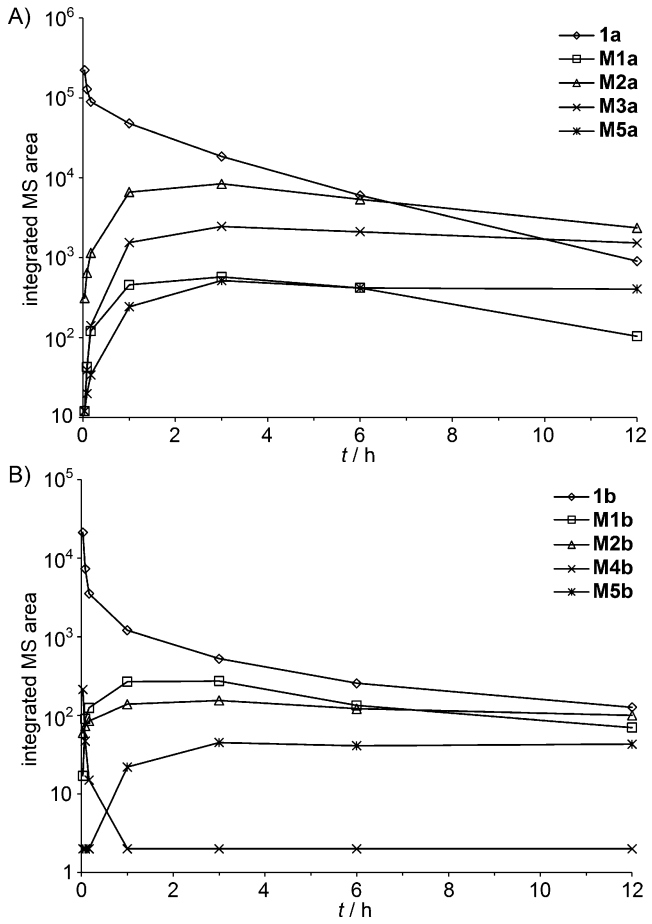

Figure 4. A) PK profiles of compound **1a** and its metabolites identified in rat plasma following i.v. administration of **1a** at 5.5 μmol kg^{-1}. B) PK profiles of compound **1b** and its metabolites identified in rat plasma following i.v. administration of **1b** at 5.1 μmol kg^{-1}.

of the later time points in Figure 4 allows a rough estimation of their clearance, which, for these metabolites, appears to be similar to or slightly lower than that of the parent drugs (**1a**, $CL = 30$ mL min^{-1} kg^{-1}; **1b**, $CL = 27$ mL min^{-1} kg^{-1}). Hydroxylation on the *N*-methyl moiety of **M2a**/**M2b** is the origin of the minor in vitro metabolite **M3a**/**M3b**. Whereas **M3a** was a major metabolite in the circulation, the corresponding sila-analogue **M3b** was not detected in the plasma. One possible reason for this difference is that **M3b** is not formed in vivo. On a more speculative note, **M3b**, in contrast to **M3a**, could be a good substrate for active transport into urine and/or bile. The third major metabolite of sila-loperamide in the in vitro experiments, silanediol **M4b**, formed presumably via hydroxylation on the silapiperidine moiety at the α-position to the nitrogen atom followed by hydrolytic ring opening, was also detected in vivo as a major metabolite at the early time points. In contrast to the relatively stable metabolites **M1b** and **M2b**, metabolite **M4b** displayed a completely different PK profile and was rapidly cleared from the circulation. There could be several reasons for such a PK profile: rapid elimination of **M4b** into urine and/or bile or metabolism to secondary metabolites that could not be detected with the applied LC–MS conditions. The pyridinium-type metabolite **M4a** was not observed in vivo, whereas relatively low levels of the minor in vitro metabolites **M5a** and **M5b** were detected.

Under the assumption that the *AUC* of the PK profiles in Figure 4 reflect, to some extent, the concentration over time and number of the main metabolites in the body, it appears that the burden of the metabolites of sila-loperamide in the blood is lower than that of the main metabolites of loperamide.

Conclusions

Sila-loperamide (**1b**), a silicon analogue of the opioid receptor agonist loperamide (**1a**), was prepared in a multistep synthesis, starting from triethoxyvinylsilane. In this synthesis, the use of the 4-methoxyphenyl (MOP) moiety as a protecting group for silicon played a key role. The physicochemical properties of the C/Si analogues **1a** and **1b** were found to be nearly identical. The PD profiles of **1a** and **1b** were studied at the human μ1 opioid and rat κ1 opioid receptors. Both compounds exhibited sub-nanomolar binding affinities and agonist potency at the μ1 receptor, which is the primary target of loperamide. The compounds are full agonists at both receptors studied. Significant differences were observed in their ability to permeate Caco-2 cell membranes, where sila-loperamide showed lower permeability and a higher efflux ratio than loperamide. Both compounds are strong substrates for the P-gp transporter (MDR1/ABCB1). Clearance in human and rat hepatocytes is not limited by the low permeability of **1a** and **1b**. Loperamide and sila-loperamide are both readily oxidized in human liver microsomes. The CRP profile of both compounds confirms that the CYP3A4 isoform is the main enzyme responsible for metabolic clearance in vitro. No time-dependent CYP inhibition was observed, and the CYP inhibitory potency was found to be < 1 μM only for CYP2D6. The in vivo PK profile of the C/Si analogues **1a** and **1b** was studied in male Han Wistar rats and compared with available published data for **1a**. Basic PK parameters such as clearance (*CL*), volume of distribution (V_{ss}), p.o. and i.v. half-life ($t_{1/2}$), and oral bioavailability (*F*) were similar for both drugs. However, the lower unbound fraction of sila-loperamide in the plasma protects **1b** from elimination, whereas the CL_u value is much higher for **1b** than for **1a**. Ultimately, this leads to lower $C_{u,max}$ and AUC_u values for **1b** than for **1a**. The combination of increased efflux ratio and decreased permeability and C_u observed for **1b** might result in a decreased exposure of **1b** into the CNS and increased safety margins. Furthermore, there are marked differences in the in vitro and in vivo metabolite pattern between loperamide and sila-loperamide. Whereas two main in vivo metabolites (**M1a**/**M1b**, **M2a**/**M2b**) and one minor in vivo metabolite (**M5a**/**M5b**) for **1a** and **1b** represent C/Si analogues, the formation of the sila-analogue of the metabolite **M3a** was not observed. Instead, sila-loperamide forms a third main metabolite, silanediol **M4b**. This metabolite is readily cleared in vivo, whereas the three other less polar metabolites have much longer half-lives. This demonstrates that sila-loperamide has access to different metabolic biotransformations, leading to an altered elimination

compared to the parent carbon compound loperamide, thereby decreasing the overall burden of formed metabolites over time. Interestingly, no conjugate formation in hepatocytes or in vivo was observed for either **1a** or **1b**.

In summary, it is increasingly unlikely in today's market environment that a carbon/silicon switch would replace a safe and inexpensive drug. However, with improved synthetic access to organosilicon compounds and a better understanding of their physicochemical and PK and PD properties in vitro and in vivo, organosilicon compounds can be successfully used to modify several properties using smart drug design. For example, it is possible to introduce metabolic soft spots, avoid formation of reactive glucuronides, and alter the in vivo pharmacology (in this context, see also reference [31]). Although carbon/oxygen or carbon/nitrogen switches are well-established approaches in medicinal chemistry, the carbon/silicon switch offers an additional option with a much higher probability of retaining PD activity than the other switches, due to more subtle changes in structural and electronic properties. On the other hand, differences in metabolic pathways and changes in the PK properties can be significant, given the different chemical properties of C/Si analogues. Our data provide clear evidence that the carbon/silicon switch strategy is more than a "patent busting" activity; it is a powerful tool to improve the overall properties of drugs. In answer to the title question: Silicon *can* make an excellent drug even better.

Experimental Section

Chemistry

General procedures: All syntheses involving chemicals sensitive to water and/or oxygen were carried out under a dry argon atmosphere. The organic solvents used were dried and purified according to standard procedures and stored under dry nitrogen. High-pressure liquid chromatography (HPLC) was performed by using a Gilson Preparative HPLC with a gradient pump system 333/334, GX-281 injector, and UV/Vis detector 155. Bulb-to-bulb distillations were carried out with a Büchi GKR-50 Glass Oven apparatus. Lyophilization was performed with a Christ alpha 1-2 apparatus. ^{1}H, ^{13}C, and ^{29}Si NMR spectra were recorded at 23 °C on Bruker DRX-300 [compound **5** (^{1}H, 300.1 MHz; ^{13}C, 75.5 MHz; ^{29}Si, 59.6 MHz)], Bruker Avance 500 [compounds **3**, **4**, **6**, **7**·HCl, and **9** (^{1}H, 500.1 MHz; ^{13}C, 125.8 MHz; ^{29}Si, 99.4 MHz)], or Bruker Avance III NMR spectrometers [compound **1b** (^{1}H, 500.0 MHz; ^{13}C, 125.7 MHz; ^{29}Si, 99.3 MHz)] using CD_2Cl_2, $CDCl_3$, C_6D_6, or [D$_6$]DMSO as solvent. Chemical shifts (δ, ppm) were determined relative to internal $CHDCl_2$ (^{1}H, $\delta = 5.32$ ppm; CD_2Cl_2), internal CD_2Cl_2 (^{13}C, $\delta = 53.8$ ppm; CD_2Cl_2), internal $CHCl_3$ (^{1}H, $\delta = 7.24$ ppm; $CDCl_3$), internal $CDCl_3$ (^{13}C, $\delta = 77.0$ ppm; $CDCl_3$), internal C_6HD_5 (^{1}H, $\delta = 7.28$ ppm; C_6D_6), internal C_6D_6 (^{13}C, $\delta = 128.0$ ppm; C_6D_6), internal [D$_5$]DMSO (^{1}H, $\delta = 2.49$ ppm; [D$_6$]DMSO), internal [D$_6$]DMSO (^{13}C, $\delta = 39.5$ ppm; [D$_6$]DMSO), and external TMS (^{29}Si, $\delta = 0.0$ ppm; CD_2Cl_2, $CDCl_3$, C_6D_6, [D$_6$]DMSO). Analysis and assignment of the ^{1}H NMR spectroscopic data were supported by ^{1}H,^{1}H gradient-selected COSY, ^{13}C,^{1}H gradient-selected HMQC, and ^{13}C,^{1}H gradient-selected HMBC experiments. Assignment of the ^{13}C NMR spectroscopic data was supported by DEPT-135 and the aforementioned ^{13}C,^{1}H correlation experiments. Coupling constants are given as their absolute values. Elemental analyses were performed with a VarioMicro apparatus (Elementar Analysensysteme GmbH) or a EURO EA Elemental Analyzer (Euro Vector). High-resolution mass spectra (HRMS, ESI+) were recorded on a Waters LCTP mass spectrometer using solutions in DMSO.

4-(4-Chlorophenyl)-1-(4-dimethylamino-4-oxo-3,3-diphenylbutyl)-4-hydroxy-4-silapiperidine (sila-loperamide 1b): Trifluoromethanesulfonic acid (153 mg, 1.02 mmol) was added dropwise at 0 °C within 1 min to a stirred solution of **9** (300 mg, 514 μmol) in CH_2Cl_2 (15 mL), and the mixture was stirred at 0 °C for 30 min and then at 20 °C for a further 30 min. Subsequently, the mixture was cooled to 0 °C, triethylammonium chloride (200 mg, 1.45 mmol) was added in a single portion, and the mixture was stirred at 0 °C for 30 min. The solvent was removed under reduced pressure, THF (15 mL) was added to the stirred residue at 20 °C, and the mixture was then kept undisturbed at −18 °C for 2 h. The upper layer of the resulting two-phase system was separated from the lower layer (triethylammonium trifluoromethanesulfonate) by means of a syringe and cooled to 0 °C. To this solution, MeOH (200 mg, 6.24 mmol) and Et_3N (500 mg, 4.94 mmol) were added sequentially in single portions, and the mixture was stirred at 0 °C for 30 min and then kept undisturbed at −18 °C for 16 h. The resulting precipitate was filtered off and discarded, and the solvent, excess MeOH, excess Et_3N, and anisole (formed in the Si–C cleavage reaction) were removed from the filtrate under reduced pressure in a bulb-to-bulb distillation apparatus to yield 4-(4-chlorophenyl)-1-(4-dimethylamino-4-oxo-3,3-diphenylbutyl)-4-methoxy-4-silapiperidine (**10**) as an oily crude product. This product was dissolved in CH_3CN (5 mL), and a 1 M ethereal HCl solution (1.0 mL, 1.0 mmol of HCl) was added at 20 °C, immediately followed by the addition of H_2O (1.0 mL). The solvents were removed under reduced pressure, the residue was dissolved in CH_2Cl_2 (10 mL), and the resulting solution was washed sequentially with H_2O (10 mL) and a 1 M aqueous solution of NaOH (10 mL). The aqueous extracts were discarded, the organic extract was dried over anhydrous Na_2SO_4, and the solvent was removed under reduced pressure to furnish **1b** as a crude product, which was dissolved in DMSO (1.0 mL) and then purified by preparative HPLC on silica gel (XBridge C_{18} column; 10 μm, 250×19 mm) using a gradient of 45–85% CH_3CN in H_2O/CH_3CN/NH_3 (95:5:0.2 *v/v/v*) buffer over 20 min (flow rate: 19 mL min^{-1}, detector λ: 220 nm). The relevant fractions were combined and freeze-dried to give **1b** as a colorless powder (79 mg, 160 μmol; 31%). ^{1}H NMR ([D$_6$]DMSO): $\delta = 0.67$–0.75 and 0.77–0.87 (m, 4H, SiCH_2CH$_2$N), 1.99–2.08 (m, 2H, NCH$_2$CH_2C), 2.24 (br s, 3H, NCH_3), 2.25–2.34 (m, 2H, NCH_2CH$_2$C), 2.50–2.56 and 2.57–2.64 (m, 4H, SiCH$_2$CH_2N), 2.85 (br s, 3H, NCH_3), 6.07 (s, 1H, SiO*H*), 7.24–7.42 and 7.48–7.50 ppm (m, 14H, C_6H_5, C_6H_4Cl); ^{13}C NMR ([D$_6$]DMSO): $\delta =$ 14.0 (SiCH_2CH$_2$N), 36.6 (NCH$_3$), 38.5 (NCH$_3$), 41.4 (NCH$_2$CH$_2$C), 51.6 (SiCH$_2$CH$_2$N), 54.2 (NCH$_2$CH$_2$C), 58.9 (NCH$_2$CH$_2$*C*), 126.5 (C4, C_6H_5), 127.69 (C3/C5, C_6H_4Cl), 127.73 (C3/C5, C_6H_5), 128.3 (C2/C6, C_6H_5), 134.4 (C1, C_6H_4Cl), 135.2 (C2/C6, C_6H_4Cl), 137.1 (C4, C_6H_4Cl), 141.1 (C1, C_6H_5), 172.2 ppm (C=O); ^{29}Si NMR ([D$_6$]DMSO): $\delta = -6.8$ ppm; HRMS (ESI): $C_{28}H_{33}ClN_2O_2Si$ $[M+H]^+$, calcd: 493.2100; found: 493.2079.

Triethoxyvinylsilane (2): This compound was commercially available.

(4-Chlorophenyl)diethoxyvinylsilane (3): A 1 M solution of (4-chlorophenyl)magnesium bromide in Et_2O (800 mL, 800 mmol of 4-ClC_6H_4MgBr) was added dropwise at 0 °C within 4 h to a stirred solution of **2** (457 g, 2.40 mol) in Et_2O (800 mL), and the mixture was then stirred at 20 °C for 16 h. Subsequently, the mixture was concentrated under reduced pressure to a volume of ~500 mL, followed by the addition of *n*-pentane (800 mL). The resulting sus-

pension was stirred at 20 °C for 10 min, the precipitate was removed by filtration and washed with *n*-pentane (3×100 mL), and the solvent of the filtrate (including the wash solutions) was removed under reduced pressure. The excess of **2** was separated from the residue by distillation in vacuo (34 mbar, 69 °C), and the residue was then further distilled in vacuo (1 mbar, 78 °C) to give **3** as a colorless liquid (169 g, 658 mmol, 82%). ^{1}H NMR ($CDCl_3$): δ = 1.28 (δ_X), 3.86 (δ_A), and 3.88 (δ_B) (ABX_3 system, $^2J_{AB}$ = 10.3 Hz, $^3J_{AX}$ = 6.8 Hz, $^3J_{BX}$ = 7.2 Hz, 10H, $OCH_AH_BC(H_X)_3$), 5.94 (δ_A), 6.12 (δ_M), and 6.22 (δ_X) (AMX system, $^2J_{AM}$ = 4.6 Hz, $^3J_{A(E)X}$ = 14.7 Hz, $^3J_{M(Z)X}$ = 19.8 Hz, 3H, $CH_X{=}CH_AH_M$), 7.38–7.41 (m, 2H, *H*-2/*H*-6, C_6H_4Cl), 7.60–7.64 ppm (m, 2H, *H*-3/*H*-5, C_6H_4Cl); ^{13}C NMR ($CDCl_3$): δ = 18.3 (OCH_2CH_3), 58.8 (OCH_2CH_3), 128.1 (C2/C6, C_6H_4Cl), 131.5 (C1, C_6H_4Cl), 131.7 ($CH{=}CH_2$), 136.0 (C3/C5, C_6H_4Cl), 136.6 (C4, C_6H_4Cl), 137.3 ppm ($CH{=}CH_2$); ^{29}Si NMR ($CDCl_3$): δ = −33.2 ppm; anal. calcd (%) for $C_{12}H_{17}ClO_2Si$ (256.80): C 56.13, H 6.67; found: C 56.33, H 6.75.

(4-Chlorophenyl)(4-methoxyphenyl)divinylsilane (4): A 0.5 M solution of (4-methoxyphenyl)magnesium bromide in THF (624 mL, 312 mmol of 4-$MeOC_6H_4MgBr$) was added dropwise at 20 °C within 3 h to a stirred solution of **3** (80.0 g, 312 mmol) in Et_2O (800 mL), and the mixture was then stirred at 20 °C for 16 h. Subsequently, a 0.7 M solution of vinylmagnesium chloride in THF (491 mL, 344 mmol of $CH_2{=}CHMgCl$) was added dropwise at 20 °C within 2 h, and the mixture was heated under reflux for 16 h. The mixture was then concentrated under reduced pressure to a volume of ~200 mL, followed by sequential addition of Et_2O (500 mL) and a saturated aqueous Na_2CO_3 solution (200 mL) at 0 °C. The organic layer was separated, the aqueous layer was extracted with Et_2O (3×100 mL) and discarded, the combined organic extracts were dried over anhydrous Na_2SO_4, the solvent was removed under reduced pressure, and the residue was purified by bulb-to-bulb distillation in vacuo (1 mbar, 180 °C) to give **4** as a colorless liquid (80.0 g, 266 mmol, 86%). ^{1}H NMR (CD_2Cl_2): δ = 3.81 (s, 3H, $C_6H_4OCH_3$), 5.79 (δ_A), 6.27 (δ_M), and 6.48 (δ_X) (AMX system, $^2J_{AM}$ = 3.7 Hz, $^3J_{A(E)X}$ = 14.6 Hz, $^3J_{M(Z)X}$ = 20.2 Hz, 6H, $CH_X{=}CH_AH_M$), 6.92–6.95 (m, 2H, *H*-2/*H*-6, $C_6H_4OCH_3$), 7.35–7.38 (m, 2H, *H*-2/*H*-6, C_6H_4Cl), 7.43–7.46 (m, 2H, *H*-3/*H*-5, C_6H_4Cl), 7.46–7.48 ppm (m, 2H, *H*-3/*H*-5, $C_6H_4OCH_3$); ^{13}C NMR (CD_2Cl_2): δ = 55.4 ($C_6H_4OCH_3$), 114.1 (C2/C6, $C_6H_4OCH_3$), 124.6 (C1, $C_6H_4OCH_3$), 128.4 (C2/C6, C_6H_4Cl), 133.8 (C1, C_6H_4Cl), 134.1 ($CH{=}CH_2$), 136.1 (C4, C_6H_4Cl), 136.8 ($CH{=}CH_2$), 137.2 (C3/C5, C_6H_4Cl), 137.3 (C3/C5, $C_6H_4OCH_3$), 161.5 ppm (C4, $C_6H_4OCH_3$); ^{29}Si NMR (CD_2Cl_2): δ = −20.9 ppm; anal. calcd (%) for $C_{17}H_{17}ClOSi$ (300.86): C 67.87, H 5.70; found: C 67.80, H 5.80.

(4-Chlorophenyl)bis(2-hydroxyethyl)(4-methoxyphenyl)silane (5): A solution of 9-borabicyclo[3.3.1]nonane [63.1 g, 259 mmol (based on the 9-BBN dimer)] and **4** (70.0 g, 233 mmol) in THF (1 L) was stirred at 20 °C for 16 h, followed by sequential addition of H_2O (200 mL) and a 4 M aqueous NaOH solution (300 mL, 1.20 mol of NaOH) at 0 °C. Subsequently, an aqueous H_2O_2 solution (30 wt%, 420 mL) was added dropwise at 0 °C within 4 h to the stirred reaction mixture, which was then heated under reflux for 3 h, followed by sequential addition of a 0.1 M aqueous solution of K_2CO_3 (500 mL) and CH_2Cl_2 (500 mL) at 20 °C. The organic layer was separated, the aqueous layer was extracted with CH_2Cl_2 (3×200 mL) and discarded, the combined organic extracts were dried over anhydrous Na_2SO_4, and the solvent was removed under reduced pressure to give a colorless oil. The byproduct cyclooctane-1,5-diol was separated from this crude product by bulb-to-bulb distillation (0.07 mbar, 160 °C), and the residue was then purified by column chromatography on aluminum oxide [Al_2O_3, Brockmann III; eluent, *n*-hexane/CH_2Cl_2/EtOH (20:50:4 *v*/*v*/*v*)]. The relevant fractions were combined, and the solvents were removed under reduced pressure to give **5**, after crystallization from Et_2O at 20 °C, as a colorless crystalline solid (71.2 g, 211 mmol, 91%). ^{1}H NMR (C_6D_6): δ = 1.30–1.35 (m, 4H, CH_2CH_2OH), 1.53 (s, 2H, CH_2CH_2OH), 3.32 (s, 3H, $C_6H_4OCH_3$), 3.57–3.62 (m, 4H, CH_2CH_2OH), 6.82–6.85 (m, 2H, *H*-2/*H*-6, $C_6H_4OCH_3$), 7.16–7.18 (m, 2H, *H*-2/*H*-6, C_6H_4Cl), 7.21–7.25 (m, 2H, *H*-3/*H*-5, C_6H_4Cl), 7.31–7.35 ppm (m, 2H, *H*-3/*H*-5, $C_6H_4OCH_3$); ^{13}C NMR (C_6D_6): δ = 18.4 (CH_2CH_2OH), 54.6 (CH_2CH_2OH), 59.2 ($C_6H_4OCH_3$), 114.2 (C2/C6, $C_6H_4OCH_3$), 125.8 (C1, $C_6H_4OCH_3$), 128.4 (C1, C_6H_4Cl), 134.9 (C4, C_6H_4Cl), 136.0 (C2/C6, C_6H_4Cl), 136.58 (C3/C5, C_6H_4Cl), 136.59 (C3/C5, $C_6H_4OCH_3$), 161.4 ppm (C4, $C_6H_4OCH_3$); ^{29}Si NMR (C_6D_6): δ = −9.3 ppm; anal. calcd (%) for $C_{17}H_{21}ClO_3Si$ (336.89): C 60.61, H 6.28; found: C 60.98, H 6.25.

1-Allyl-4-(4-chlorophenyl)-4-(4-methoxyphenyl)-4-silapiperidine (6): Methanesulfonyl chloride (17.1 g, 149 mmol) and Et_3N (18.0 g, 178 mmol) were added sequentially in single portions at −20 °C to a stirred solution of **5** (20.0 g, 59.4 mmol) in CH_2Cl_2 (500 mL), and the mixture was then stirred at −20 °C for 3 h. Subsequently, allylamine (100 g, 1.75 mol) was added in a single portion at −20 °C to the mixture, which was then warmed to 20 °C and stirred at 20 °C for 16 h. The solvent and excess allylamine were removed from the reaction mixture under reduced pressure, followed by sequential addition of EtOAc (200 mL) and a saturated aqueous $NaHCO_3$ solution (100 mL) at 20 °C. The organic layer was separated, the aqueous layer was extracted with EtOAc (3×50 mL) and discarded, the combined organic extracts were dried over anhydrous Na_2SO_4, and the solvent was removed under reduced pressure to give an oily residue. This crude product was dissolved in Et_2O (100 mL), and a 2 M ethereal HCl solution (33.0 mL, 66.0 mmol of HCl) was added dropwise at 20 °C within 5 min. The resulting precipitate was isolated by filtration and recrystallized from 2-propanol (50 mL) by slow cooling of the boiling solution to 20 °C. The product was isolated by filtration and washed with Et_2O (2×10 mL) to give **6**·HCl as a colorless crystalline solid, which was subsequently added in a single portion at 20 °C to a stirred two-phase system consisting of a 2 M aqueous NaOH solution (33.0 mL, 66.0 mmol of NaOH) and Et_2O (200 mL), and the mixture was then stirred at 20 °C for 30 min, followed by the addition of H_2O (200 mL). The organic layer was separated, the aqueous layer was extracted with Et_2O (3×50 mL) and discarded, the combined organic extracts were dried over anhydrous Na_2SO_4, and the solvent was removed under reduced pressure to give **6** as a colorless oil (8.52 g, 23.8 mmol, 40%). ^{1}H NMR (CD_2Cl_2): δ = 1.26–1.35 (m, 4H, $SiCH_2CH_2N$), 2.71–2.80 (m, 4H, $SiCH_2CH_2N$), 3.03–3.06 (m, 2H, $CH_2CH{=}CH_2$), 3.80 (s, 3H, $C_6H_4OCH_3$), 5.07–5.11 and 5.12–5.17 (m, 2H, $CH_2CH{=}CH_2$), 5.82–5.90 (m, 1H, $CH_2CH{=}CH_2$), 6.90–6.94 (m, 2H, *H*-2/*H*-6, $C_6H_4OCH_3$), 7.33–7.36 (m, 2H, *H*-2/*H*-6, C_6H_4Cl), 7.42–7.45 (m, 2H, *H*-3/*H*-5, C_6H_4Cl), 7.46–7.49 ppm (m, 2H, *H*-3/*H*-5, $C_6H_4OCH_3$); ^{13}C NMR (CD_2Cl_2): δ = 11.8 ($SiCH_2CH_2N$), 52.4 ($SiCH_2CH_2N$), 55.4 ($C_6H_4OCH_3$), 61.9 ($NCH_2CH{=}CH_2$), 114.1 (C2/C6, $C_6H_4OCH_3$), 117.0 ($NCH_2CH{=}CH_2$), 126.1 (C1, $C_6H_4OCH_3$), 128.4 (C2/C6, C_6H_4Cl), 135.2 (C1, C_6H_4Cl), 135.8 (C4, C_6H_4Cl), 136.42 (C3/C5, C_6H_4Cl), 136.43 (C3/C5, $C_6H_4OCH_3$), 136.6 ($NCH_2CH{=}CH_2$), 161.3 ppm (C4, $C_6H_4OCH_3$); ^{29}Si NMR (CD_2Cl_2): δ = −15.6 ppm; anal. calcd (%) for $C_{20}H_{24}ClNOSi$ (357.95): C 67.11, H 6.76, N 3.91; found: C 66.80, H 6.80, N 3.91.

4-(4-Chlorophenyl)-4-(4-methoxyphenyl)-4-silapiperidinium chloride (7·HCl): 1-Chloroethyl chloroformate (2.32 g, 16.2 mmol) was added dropwise at 0 °C within 5 min to stirred solution of **6** (5.25 g, 14.7 mmol) in $CHCl_3$ (250 mL), and the mixture was stirred at 0 °C for 10 min and then heated under reflux for 2 h. Subsequently, the mixture was cooled to 20 °C, the solvent was removed under reduced pressure, the residue was dissolved in MeOH

(100 mL), and the resulting solution was heated under reflux for 2 h. Approximately 80 mL of MeOH were removed by distillation under atmospheric pressure, and the remaining mixture was then kept undisturbed at −20 °C over 16 h. The resulting precipitate was isolated by filtration and recrystallized from 2-propanol (10 mL) by slow cooling of the boiling solution to 20 °C. The precipitate was isolated by filtration and washed with Et_2O (2×10 mL) to give **7**·HCl as a colorless crystalline solid (3.28 g, 9.26 mmol, 63%). ^{1}H NMR (CD_2Cl_2): δ = 1.62–1.80 (m, 4H, Si$CH_2$$CH_2$N), 3.27–3.51 (m, 4H, Si$CH_2CH_2$N), 3.81 (s, 3H, $C_6H_4OCH_3$), 6.95–6.98 (m, 2H, *H*-2/*H*-6, $C_6H_4OCH_3$), 7.38–7.41 (m, 2H, *H*-2/*H*-6, C_6H_4Cl), 7.47–7.49 (m, 2H, *H*-3/*H*-5, C_6H_4Cl), 7.50–7.53 (m, 2H, *H*-3/*H*-5, $C_6H_4OCH_3$), 9.76 ppm (br s, 2H, NH_2); ^{13}C NMR (CD_2Cl_2): δ = 9.5 (SiCH_2CH_2N), 44.4 (SiCH_2CH_2N), 55.5 ($C_6H_4OCH_3$), 114.6 (C2/C6, $C_6H_4OCH_3$), 122.5 (C1, C_6H_4Cl), 128.8 (C2/C6, C_6H_4Cl), 131.9 (C1, $C_6H_4OCH_3$), 136.45 (C3/C5, C_6H_4Cl), 136.55 (C3/C5, $C_6H_4OCH_3$), 136.9 (C4, C_6H_4Cl), 162.0 ppm (C4, $C_6H_4OCH_3$); ^{29}Si NMR (CD_2Cl_2): δ = −16.9 ppm; anal. calcd (%) for $C_{17}H_{21}Cl_2NOSi$ (354.35): C 57.62, H 5.97, N 3.95; found: C 57.56, H 6.05, N 4.02.

4-(4-Chlorophenyl)-1-(4-dimethylamino-4-oxo-3,3-diphenylbutyl)-4-(4-methoxyphenyl)-4-silapiperidine (9): A mixture of **7**·HCl (2.43 g, 6.86 mmol), **8** (2.61 g, 7.54 mmol), anhydrous Na_2CO_3 (3.20 g, 30.2 mmol), and CH_3CN (200 mL) was heated under reflux for 16 h. The mixture was then cooled to 20 °C, the solvent was removed under reduced pressure, and H_2O (100 mL) and CH_2Cl_2 (100 mL) were added sequentially to the residue. The organic layer was separated, the aqueous layer was extracted with CH_2Cl_2 (3× 50 mL) and discarded, the combined organic extracts were dried over anhydrous Na_2SO_4, and the solvent was removed under reduced pressure. The solid residue was purified by column chromatography on silica gel [40–63 μm, 300 g (Merck), treated with concentrated aqueous ammonia solution (7% by weight relative to the silica gel); eluent, CH_2Cl_2/MeOH (97:3 *v/v*)]. The relevant fractions were combined, and the solvents were removed under reduced pressure to give **9** as a colorless crystalline solid (2.52 g, 4.32 mmol, 63%). ^{1}H NMR (CD_2Cl_2): δ = 1.06–1.33 (m, 4H, SiCH_2CH_2N), 2.06–2.22 (m, 2H, NCH_2CH_2C), 2.30 (br s, 3H, NCH_3), 2.36–2.52 (m, 2H, NCH_2CH_2C), 2.60–2.76 (m, 4H, SiCH_2CH_2N), 2.92 (br s, 3H, NCH_3), 3.78 (s, 3H, $C_6H_4OCH_3$), 6.87–6.90 and 7.25–7.43 ppm (m, 18H, C_6H_5, $C_6H_4OCH_3$, C_6H_4Cl); ^{13}C NMR (CD_2Cl_2): δ = 11.5 (SiCH_2CH_2N), 37.2 (NCH_3), 39.3 (NCH_3), 42.2 (NCH_2CH_2C), 52.3 (SiCH_2CH_2N), 55.3 (NCH_2CH_2C), 59.9 (NCH_2CH_2C), 114.1 (C3/C5, $C_6H_4OCH_3$), 126.2 (C1, $C_6H_4OCH_3$), 126.9 (C4, C_6H_5), 128.3 (C2/C6, C_6H_4Cl), 128.5 (C3/C5, C_6H_5), 128.6 (C2/C6, C_6H_5), 135.3 (C1, C_6H_4Cl), 135.7 (C4, C_6H_4Cl), 136.39 (C3/C5, C_6H_4Cl), 136.41 (C2/C6, $C_6H_4OCH_3$), 141.5 (C1, C_6H_5), 161.2 (C4, $C_6H_4OCH_3$), 173.3 ppm (C=O); ^{29}Si NMR (CD_2Cl_2): δ = −15.6 ppm; HRMS (ESI): $C_{35}H_{39}ClN_2O_2S$ $[M+H]^+$, calcd: 583.2548; found: 583.2558.

4-(4-Chlorophenyl)-1-(4-dimethylamino-4-oxo-3,3-diphenylbutyl)-4-methoxy-4-silapiperidine (10): This compound was isolated in the synthesis of **1b** as a crude product and was not further purified. HRMS (ESI): $C_{29}H_{35}ClN_2O_2Si$ $[M+H]^+$, calcd: 507.2235; found: 507.2212.

Physicochemical properties

log *D* values (pH 7.4): Partitioning of the test compounds between 1-octanol and 0.1 M phosphate buffer, pH 7.4, at 20 °C was determined by using a modified version of the shake-flask method described by Leo et al.[27] The compounds were dissolved, in a 96-well plate, in 400 μL of octanol, and 400 μL of buffer were added to each well. The plate was vigorously stirred for 5 min and then put on an Edmund Bühler shaker for 18 h at 20 °C. Aliquots (5 μL) of octanol were transferred and diluted with 495 μL of CH_3CN/H_2O (1:1 *v/v*) and, to avoid contamination of the buffer, the rest of the octanol was removed before 150 μL of buffer samples were transferred. Octanol and buffer samples were diluted with CH_3CN/H_2O (1:1 *v/v*) in four 10-fold steps to yield octanol samples diluted 100- to 1 000 000-fold and buffer samples diluted 1- to 10 000-fold. LC–MS/MS was used for analysis, and log *D* was calculated from the integrated peak areas of the samples in the linear MS response range.

Solubility in HBSS buffer (pH 7.4): Solutions of test compounds in DMSO (30 μL, 10 mM) in glass vials were dried using a Genevac vacuum evaporator. When samples were dry, 300 μL of 0.1 M phosphate buffer, pH 7.4, was added to the glass vials. The vials were put on an Edmund Bühler shaker for 18 h at 20 °C. Samples were filtered through a Whatman GF/B 96-well filter, and 20 μL of the filtrated samples were transferred to separate wells in a plate containing 180 μL of CH_3CN/H_2O (1:1 *v/v*). Standards were prepared by diluting the 10 mM solutions of the test compounds with CH_3CN/H_2O (1:1 *v/v*) to 200 μM. Three further 10-fold dilution steps were applied to both the samples and the standards, and they were all analyzed by LC–MS/MS. The solubility was determined by using the integrated peak areas of the samples in the linear MS response range.

pK_a values: The pK_a values were obtained according to reference [28]. The method uses pressure-assisted capillary electrophoresis (HPCE^{3D}, Agilent Technologies) coupled online with an ion trap mass spectrometer (1100 series LC/MSD trap).

In vitro pharmacology

Radioligand binding assays: Radioligand binding assays were performed at CEREP (Poitiers, France). Briefly, displacement of the radioligands by the test compounds was measured at each receptor using membrane preparations from HEK cells expressing human μ1 opioid receptors or CHO cells expressing rat κ1 opioid receptors. Membrane homogenates (16–60 μg of protein) were incubated with 1) 0.5 nmol [^{3}H]DAMGO for μ opioid receptors in the absence or presence of the test compound in a buffer containing 50 mmol of Tris·HCl (pH 7.4) and 5 mmol of $MgCl_2$ for 120 min at 22 °C or 2) 1 nmol [^{3}H]U69593 for κ opioid receptors in the absence or presence of the test compound in a buffer containing 50 mmol of Tris·HCl (pH 7.4), 10 mmol of $MgCl_2$, and 1 mmol of EDTA for 60 min at 22 °C. Nonspecific binding was determined in the presence of 10 μmol naloxone. Following incubation at 22 °C for 60 min (κ) or 120 min (μ), samples were filtered rapidly under vacuum through glass fiber filters (GF/B, Packard), pre-soaked with 0.3% PEI, and rinsed several times with an ice-cold buffer containing 50 mmol of Tris·HCl (pH 7.4) using a 96-sample cell harvester (Unifilter, Packard). The filters were dried and then counted for radioactivity in a scintillation counter (Topcount, Packard) using a scintillation cocktail (Microscint 0, Packard).

Cell-based functional assays (agonist/antagonist determination): μ and κ opioid receptor function was determined by measurement of receptor-driven inhibition of NKH 477-stimulated cAMP accumulation in HEK cells expressing human μ opioid receptors or in CHO cells expressing rat κ opioid receptors. To determine whether the test compounds were agonistic, cells were suspended in HBSS buffer (Invitrogen) complemented with 20 mmol of HEPES (pH 7.4) and 500 μmol IBMX and then distributed in microplates at a density of 7×10^3 cells per well (HEK/μ) or 10^4 cells per well (CHO/κ) and pre-incubated for 5 min at 20 °C in the presence of HBSS or the

test compounds, following which NKH 477 was added to a concentration of 10 μmol. After a further 10 min incubation at 37 °C, the cells were lysed, and the fluorescence acceptor (D2-labeled cAMP) and fluorescence donor (anti-cAMP antibody labeled with europium cryptate) were added. After 60 min at 20 °C, the fluorescence transfer was measured at the excitation wavelength 337 nm and emission wavelengths 620 and 665 nm using a microplate reader (Rubystar, BMG). The cAMP concentration was determined by dividing the signal measured at 665 nm by that measured at 620 nm (ratio) relative to a standard curve. To determine whether the test compounds had antagonistic effects, a reference agonist was added along with NKH 477: 20 nmol DAMGO for μ opioid receptors or 5 nmol U50488 for κ opioid receptors.

Data analysis: Concentration–effect data were fitted to a four-parameter logistic equation using nonlinear regression. The concentration of the test compound causing 50% maximal effect (A_{50}) for each individual curve was determined, and mean pA_{50} ($-\log A_{50}$) values were calculated with standard deviation. For radioligand binding assays, the affinity of the test compounds was estimated by the method of Cheng and Prusoff.[29]

hERG activity

Assessment of hERG blockade was made as described by Bridgland-Taylor et al.[30] CHO κ1 cells expressing hERG channels described by Persson et al.[31] were grown to semi-confluence at 37 °C in a humidified environment (5% CO_2) in Ham's F-12 nutrient mixture and L-glutamine (Sigma) supplemented with 10% fetal calf serum (Invitrogen) and 600 μg mL^{-1} hygromycin (Invitrogen). Cells were incubated at 37 °C for 24 h and then incubated at 28 °C for 48–72 h, following which a single voltage pulse was applied to evoke the pre- and post-compound hI_{ERG} currents using an IonWorks HT (Molecular Devices) platform. A holding potential of −70 mV was applied for 20 s, followed by a 160 ms step to −60 mV and a 100 ms step back to −70 mV. The voltage was then stepped to 40 mV for 1 s, and a steady-state current was observed. A 2 s step down to −30 mV, inducing the tail current, was then followed by a 0.5 s step to −70 mV. The current signal was sampled at 2.5 kHz. The hI_{ERG} current magnitude was measured automatically from the leak-subtracted traces by the IonWork software by taking a 40 ms average of the baseline current measured at −70 mV and subtracting this from the peak of the tail-current response measured during the voltage step at −30 mV. The degree of inhibition of the hI_{ERG} current was assessed by dividing the post-scan hI_{ERG} current by the respective pre-scan hI_{ERG} current for each well.

Permeability and efflux in human Caco-2 cells

A monolayer of Caco-2 cells, cultured on semi-permeable polycarbonate surfaces, was used to study the permeability in the apical-to-basolateral direction. The process was automated by a robotic Tecan EVO platform and 24-transwell plates from Costar. HBSS buffer, pH 7.4, was dispensed to the basal side of the monolayer. The assay was initiated by adding the test compound (10 μmol mL^{-1} in HBSS buffer, pH 6.5) to the apical side of the monolayer. Samples were withdrawn before the addition of the test compound and at 45 and 120 min post-addition of the test compound. During incubation, the transwell plates were placed in a shaking incubator at 37 °C between sampling. All samples were analyzed by LC–MS/MS, and the apparent permeability (P_{app}) was calculated from the peak areas. Efflux was studied in the same Caco-2 cells, with the modification that HBSS buffer, pH 7.4, was used on both sides of the monolayer. The permeability was studied in the apical-to-basolateral direction (P_{app} A→B) as well as in the basolateral-to-apical direction (P_{app} B→A). Efflux ratios were derived from the following equation: (P_{app} B→A)/(P_{app} A→B).

Permeability and efflux in MDCK-MDR1 cells

MDCK-MDR1 cells seeded onto a Millipore 96-well plate at a density of 60 000 cells per well were used to study P-gp efflux. The process was automated by a robotic Tecan EVO. HBSS buffer, pH 7.4, was dispensed to either the apical or basal side of the monolayer. The assay was initiated by adding the test substrate (1 μmol mL^{-1} in HBSS buffer, pH 7.4) to the apical or basal side of the monolayer (with HBSS buffer, pH 7.4, on the other side of the monolayer). Samples were withdrawn before the addition of the test compound and at 150 min post-addition of the test compound. During incubation, the plates were placed in a shaking incubator at 37 °C. All samples were analyzed by LC–MS/MS, and the areas were used to determine the P_{app} A→B and P_{app} B→A values. Efflux ratios were derived from the following equation: (P_{app} B→A)/(P_{app} A→B).

Intrinsic clearance and half-life in human liver microsomes and human and rat hepatocytes

Metabolic stability in human liver microsomes: Human liver microsomes were defrosted on ice and diluted to 1 mg mL^{-1} of microsomal protein in 0.1 M phosphate buffer, pH 7.4. The test compounds at 1 μM were incubated with the liver microsome suspensions and 1 mM NADPH at 37 °C in a 96-well plate. At 0.5, 5, 10, 15, 20, and 30 min, aliquots (30 μL) were transferred to a 96-well plate containing 120 μL of CH_3CN. This plate was centrifuged for 20 min, and the supernatant was removed and diluted (1:1 *v/v*) with H_2O before analysis by LC–MS/MS. Peak areas were determined from extracted ion chromatograms, and the in vitro intrinsic clearance (in vitro CL_{int}, μL min^{-1} mg^{-1} microsomal protein) of the parent compound was calculated from the slope in the regression analysis of the natural logarithm of parent concentration versus time curve.

Metabolic stability in human and male Han Wistar rat hepatocytes: Hepatocyte metabolic stability was determined in accordance with the method described by Jacobson et al.[32] Cryopreserved hepatocytes at a concentration of 10^6 viable cells per mL were used. After thawing, hepatocytes were incubated for 10 min to warm to 37 °C, and the test compound, dissolved in CH_3CN, was added to give a final concentration of 1 μM. At 0.5, 5, 15, 30, 45, 60, 80, 100, and 120 min, the incubation system was mixed, and aliquots (20 μL) were transferred at each time point to wells in a separate plate filled with 80 μL of CH_3CN to stop the reaction. The quenching plate was then vortexed, followed by centrifugation, and the supernatants were analyzed by LC–MS/MS. Peak areas were determined from extracted ion chromatograms, and the in vitro intrinsic clearance (in vitro CL_{int}, μL min^{-1} 10^6 cells) of the parent compound was calculated from the slope in the regression analysis of the natural logarithm of parent concentration versus time curve.

CYP inhibition, time-dependent CYP inhibition, and CYP reaction phenotyping

CYP inhibition: A fluorescence-based method[33] in 96-well format was used to determine the inhibition of five different CYPs (1A2, 2C9, 2D6, 3A4, and 2C19). The recombinant human enzymes used

were prepared in house, except for CYP2D6 (Cypex Ltd.). Various coumarin substrates, biotransformed into fluorescent metabolites, were used as probes for each individual CYP. A fluorescence plate reader (SpectraMax GeminiXS, Molecular Devices) was used to measure the levels of metabolites formed. A dilution series of the test compounds was prepared at eight different concentrations. For each CYP, a mixture of the enzyme, the corresponding coumarin substrate, potassium phosphate buffer (pH 7.4), and H_2O (concentrations and volumes were CYP-dependent) were added to each well in a black 96-well plate. The test compounds at different concentrations were added. After 10 min pre-incubation, the cofactor NADPH was added to initiate the reaction. After 20–50 min (CYP and substrate dependent), the reaction was terminated by the addition of Tris base/CH_3CN (20:80 *v/v*). The plates were transferred to the fluorescence plate reader, where the wavelengths were set individually for the different coumarin substrates and their respective fluorescent metabolite. The responses were exported to Microsoft Excel, in which the IC_{50} curves were plotted (percent inhibition versus concentration) and IC_{50} values calculated for each test substrate and enzyme using XL-fit.

Time-dependent CYP inhibition: Time-dependent inhibition of CYP was investigated for six CYPs (1A2, 2C8, 2C9, 2C19, 2D6, and 3A4) in a pool of human liver microsomes (1 mg mL^{-1}, BD Gentest batch 38289). The test compounds were pre-incubated at two separate concentrations (10 and 50 μM) in the presence and absence of NADPH (1 mM) for 30 min. In addition, an incubation without the test compound was performed with and without addition of NADPH. A fraction of each incubation (25 μL) was then diluted tenfold with NADPH (1 mM) and phosphate buffer (pH 7.4) containing a cocktail of probe substrates for each CYP and incubated for another 15 min. All incubations were performed in a 96-well format at 37 °C in a total volume of 250 μL using a Tecan Freedom Evo Plus 200 robot. The proteins (95 μL aliquot) were then precipitated by acidic MeOH (190 μL) and put in a freezer for 30 min, followed by centrifugation. The supernatant was transferred to a separate plate, and the response of the metabolite formation from each probe substrate was estimated by LC–MS/MS (Agilent 1100 LC and TSQ Quantum Ultra triple quadrupole mass spectrometer equipped with an APCI ion source). For each probe substrate, an LC–MS/MS response of the formed metabolite was generated in the following incubations: A) (−) test compound and (−) NADPH, B) (−) test compound and (+) NADPH, C) (−) test compound and (+) NADPH, and D) (−) test compound and (−) NADPH. The percent inhibition of compounds at both 10 and 50 μM was calculated for each CYP with the following formula: $[1-(C/D)/(B/A)]\times 100$.

CYP reaction phenotyping (CRP): The assay consisted of a panel of six recombinant cytochrome P450 (rCYP) isoforms (1A2, 2C8, 2C9, 2C19, 2D6, and 3A4; Cypex Ltd.). The incubation was performed in 96-well plates at 1 μM test compound concentration and with 50 nM rCYP at 37 °C. Aliquots for analysis by LC–MS/MS were taken at 0, 7, 15, and 30 min. Values of intrinsic clearance (CL_{int}, μL min^{-1} pmol^{-1}) were calculated for each individual rCYP. With the aid of relative activity factors derived from human liver microsomes, the rCYP CL_{int} values were then used to calculate the relative contribution by a certain CYP isoform to the total metabolism observed in the experiment.

In vivo rat PK

Two days prior to dosing, male Han Wistar rats were prepared by cannulation of the left carotid artery for blood sampling and by cannulation of the right jugular vein for intravenous (i.v.) administration. The catheters were filled with heparin (100 IU mL^{-1}), exteriorized at the nape of the neck, and sealed. The surgery was performed under isoflurane (Forene, Abbott) anesthesia. After surgery, the rats were housed individually and had free access to food and water. Approximately 16 h prior to dosing, the animals were deprived of food and fasted until 4 h after dosing. The rats had free access to drinking water during the experiment. On the experiment day, the test item formulation was administered orally by gavage or intravenously in the jugular vein. At pre-defined time points, blood samples of ~150 μL were withdrawn from the carotid artery up to 24 h after dosing. A total of 10 samples were withdrawn. The blood samples were collected in heparinized plastic tubes and centrifuged, within 30 min, for five minutes at 10000 *g* and 4 °C. The plasma was transferred to a 96-well plate and stored at −20 °C until analysis by LC–MS/MS. The studies were approved by the Göteborg Animal Research Ethical Board.

Plasma protein binding

The test compounds were added to a 96-well plate containing blood plasma to give a final concentration of 5 μM. After mixing, the samples were added to an equilibrium dialysis device (RED, Thermo Fischer Scientific Inc.) and dialyzed against phosphate buffer (0.1 M, pH 7.4) for 18 h at 37 °C. Standard curves used for quantification were prepared in plasma in a concentration range of 7 μM to 1.4 nM. Standard curve samples and dialysis samples were precipitated with CH_3CN, and after centrifugation, supernatants were analyzed by LC–MS/MS. The fraction unbound in the incubation was calculated as the concentration in the media buffer sample divided by the concentration in the plasma sample.

Identification of major in vitro metabolites and reactive metabolites

The experimental setup for metabolite identification in hepatocytes was the same as for the determination of the metabolic stability, with the following modifications: The test compound concentration was 4 μM, and the reaction was stopped by the addition of cold CH_3CN/H_2O (3:1 *v/v*). Samples for metabolite identification were taken after 40 min incubation. In addition, a blank sample without test compound was analyzed. The samples were analyzed by ultra-performance liquid chromatography (Waters ACQUITY UPLC) coupled to a Xevo G2S TOF instrument equipped with an electrospray interface. The software used to process the data was MetaboLynx (Waters). Product ion spectra of the major metabolites were acquired to allow interpretation and structural assignments.

Identification of major in vivo metabolites in plasma from male Han Wistar rats

Plasma samples from the in vivo rat PK experiments were analyzed with respect to metabolites as well as parent drug to allow the generation of metabolic profiles. To 50 μL of plasma was added 150 μL of CH_3CN to precipitate plasma proteins. The samples were vortexed for 10 s and then centrifuged for 10 min at 4 °C at ~2750 *g*. The supernatants were diluted 1:1 with 0.1% formic acid prior to analysis by ultra-performance liquid chromatography (Waters ACQUITY UPLC) coupled to a Waters Xevo G2S TOF instrument equipped with an electrospray interface. The software used to process the data was MetaboLynx (Waters). Product ion spectra of the major metabolites were acquired to allow interpretation and structural assignments.

Acknowledgements

The following people at AstraZeneca R&D are gratefully acknowledged for their work on the various biological studies and DMPK assays: Lyn Rosenbrier-Ribeiro, Malin Forsgard, Johan Wernevik, Siavash Tavakoli, Linda Fredlund, Alan Clark, Neil Shearer, Sara Amberntsson, Martina Furasen, and Charlotta Vedin.

Keywords: C/Si exchange · metabolic fate · opioid receptors · sila-drugs · silicon

[1] R. A. Stokbroekx, J. Vandenberk, A. H. M. T. Van Heertum, G. M. L. W. van Laar, M. J. M. C. Van der Aa, W. F. M. Van Bever, P. A. J. Janssen, *J. Med. Chem.* **1973**, *16*, 782 – 786.

[2] Reviews dealing with silicon-based drugs: a) R. Tacke, H. Linoh in *The Chemistry of Organic Silicon Compounds, Part 2* (Eds.: S. Patai, Z. Rappoport), Wiley, Chichester, **1989**, pp. 1143 – 1206; b) W. Bains, R. Tacke, *Curr. Opin. Drug Discovery Dev.* **2003**, *6*, 526 – 543; c) G. A. Showell, J. S. Mills, *Drug Discovery Today* **2003**, *8*, 551 – 556; d) J. S. Mills, G. A. Showell, *Expert Opin. Invest. Drugs* **2004**, *13*, 1149 – 1157; e) P. K. Pooni, G. A. Showell, *Mini-Rev. Med. Chem.* **2006**, *6*, 1169 – 1177; f) S. McN. Sieburth, C.-A. Chen, *Eur. J. Org. Chem.* **2006**, 311 – 322; g) S. Gately, R. West, *Drug Dev. Res.* **2007**, *68*, 156 – 163; h) A. K. Franz, *Curr. Opin. Drug Discovery Dev.* **2007**, *10*, 654 – 671; i) N. A. Meanwell, *J. Med. Chem.* **2011**, *54*, 2529 – 2591; j) A. K. Franz, S. O. Wilson, *J. Med. Chem.* **2013**, *56*, 388 – 405; k) S. McN. Sieburth, *Top. Med. Chem.* **2014**, DOI: 10.1007/7355_2014_80; l) R. Tacke, S. Dörrich, *Top. Med. Chem.* **2014**, DOI: 10.1007/7355_2014_55.

[3] Recent original publications dealing with silicon-based drugs: a) R. Tacke, F. Popp, B. Müller, B. Theis, C. Burschka, A. Hamacher, M. U. Kassack, D. Schepmann, B. Wünsch, U. Jurva, E. Wellner, *ChemMedChem* **2008**, *3*, 152 – 164; b) R. Tacke, B. Nguyen, C. Burschka, W. P. Lippert, A. Hamacher, C. Urban, M. U. Kassack, *Organometallics* **2010**, *29*, 1652 – 1660; c) T. Johansson, L. Weidolf, F. Popp, R. Tacke, U. Jurva, *Drug Metab. Dispos.* **2010**, *38*, 73 – 83; d) M. J. Barnes, C. Burschka, M. W. Büttner, R. Conroy, J. O. Daiss, I. C. Gray, A. G. Hendrick, L. H. Tam, D. Kuehn, D. J. Miller, J. S. Mills, P. Mitchell, J. G. Montana, P. A. Muniandy, H. Rapley, G. A. Showell, D. Tebbe, R. Tacke, J. B. H. Warneck, B. Zhu, *ChemMedChem* **2011**, *6*, 2070 – 2080; e) R. Tacke, R. Bertermann, C. Burschka, S. Dörrich, M. Fischer, B. Müller, G. Meyerhans, D. Schepmann, B. Wünsch, I. Arnason, R. Bjornsson, *ChemMedChem* **2012**, *7*, 523 – 532; f) J. B. G. Gluyas, C. Burschka, S. Dörrich, J. Vallet, H. Gronemeyer, R. Tacke, *Org. Biomol. Chem.* **2012**, *10*, 6914 – 6929; g) P. Luger, M. Weber, C. Hübschle, R. Tacke, *Org. Biomol. Chem.* **2013**, *11*, 2348 – 2354.

[4] Synthesis of 9-BBN: J. A. Soderquist, H. C. Brown, *J. Org. Chem.* **1981**, *46*, 4599 – 4600.

[5] 1-Chloroethyl chloroformate as an *N*-dealkylation agent: R. A. Olofson, J. T. Martz, J.-P. Senet, M. Piteau, T. Malfroot, *J. Org. Chem.* **1984**, *49*, 2081 – 2082.

[6] Synthesis of **8**: Z. Chen, E. Davies, W. S. Miller, S. Shan, K. J. Valenzano, D. J. Kyle, *Bioorg. Med. Chem. Lett.* **2004**, *14*, 5275 – 5279.

[7] D. L. DeHaven-Hudkins, L. C. Burgos, J. A. Cassel, J. D. Daubert, R. N. Dehaven, E. Mansson, H. Nagasaka, G. Yu, T. Yaksh, *J. Pharmacol. Exp. Ther.* **1999**, *289*, 494 – 502.

[8] S. Grimwood, P. R. Hartig, *Pharmacol. Ther.* **2009**, *122*, 281 – 301.

[9] C. E. Pollard, N. Abi Gerges, M. H. Bridgland-Taylor, A. Easter, T. G. Hammond, J.-P. Valentin, *Br. J. Pharmacol.* **2010**, *159*, 12 – 21.

[10] J. Vandenbossche, M. Huisman, Y. Xu, D. Sanderson-Bongiovanni, P. Soons, *J. Pharm. Pharmacol.* **2010**, *62*, 401 – 412.

[11] M. J. Zamek-Gliszczynski, D. W. Bedwell, J. Q. Bao, J. W. Higgins, *Drug Metab. Dispos.* **2012**, *40*, 1825 – 1833.

[12] G. Mukwaya, T. MacGregor, D. Hoelscher, T. Heming, D. Legg, K. Kavanaugh, P. Johnson, J. P. Sabo, S. McCallister, *Antimicrob. Agents Chemother.* **2005**, *49*, 4903 – 4910.

[13] K.-A. Kim, J. Chung, D.-H. Jung, J.-Y. Park, *Eur. J. Clin. Pharmacol.* **2004**, *60*, 575 – 581.

[14] J. A. Williams, B. J. Ring, V. E. Cantrell, D. R. Jones, J. Eckstein, K. Ruterbories, M. A. Hamman, S. D. Hall, S. A. Wrighton, *Drug Metab. Dispos.* **2002**, *30*, 883 – 891.

[15] P. L. Toutain, A. Bousquet-Mélou, *J. Vet. Pharmacol. Ther.* **2004**, *27*, 415 – 425.

[16] J. D. O'Brien, D. G. Thompson, A. McIntyre, W. R. Burnham, E. Walker, *Gut* **1988**, *29*, 312 – 318.

[17] J. Heykants, M. Michiels, A. Knaeps, J. Brugmans, *Arzneim.-Forsch.* **1974**, *24*, 1649 – 1653.

[18] Z. Zhivkova, I. Doytchinova, *Mol. Pharm.* **2013**, *10*, 3758 – 3768.

[19] D. A. Smith, L. Di, E. H. Kerns, *Nat. Rev. Drug Discovery* **2010**, *9*, 929 – 939.

[20] L. Huang, L. Berry, S. Ganga, B. Janosky, A. Chen, J. Roberts, A. E. Colletti, M.-H. J. Lin, *Drug Metab. Dispos.* **2010**, *38*, 223 – 231.

[21] K. Ito, J. B. Houston, *Pharm. Res.* **2004**, *21*, 785 – 792.

[22] A.-K. Sohlenius-Sternbeck, C. Jones, D. Ferguson, B. J. Middleton, D. Projean, E. Floby, J. Bylund, L. Afzelius, *Xenobiotica* **2012**, *42*, 841 – 853.

[23] R. N. Upton, *Clin. Exp. Pharmacol. Physiol.* **2007**, *34*, 695 – 701.

[24] A. S. Kalgutkar, H. T. Nguyen, *Drug Metab. Dispos.* **2004**, *32*, 943 – 952.

[25] K. Igarashi, F. Kasuya, E. Usuki, N. Castagnoli, Jr., *Life Sci.* **1995**, *57*, 2439 – 2446.

[26] E. Usuki, R. Pearce, A. Parkinson, N. Castagnoli, Jr., *Chem. Res. Toxicol.* **1996**, *9*, 800 – 806.

[27] A. Leo, C. Hansch, D. Elkins, *Chem. Rev.* **1971**, *71*, 525 – 615.

[28] H. Wan, A. G. Holmén, Y. Wang, W. Lindberg, M. Englund, M. B. Någård, R. A. Thompson, *Rapid Commun. Mass Spectrom.* **2003**, *17*, 2639 – 2648.

[29] Y.-C. Cheng, H. W. Prusoff, *Biochem. Pharmacol.* **1973**, *22*, 3099 – 3108.

[30] M. H. Bridgland-Taylor, A. C. Hargreaves, A. Easter, A. Orme, D. C. Henthorn, M. Ding, A. M. Davis, B. G. Small, C. G. Heapy, N. Abi-Gerges, F. Persson, I. Jacobson, M. Sullivan, N. Albertson, T. G. Hammond, E. Sullivan, J.-P. Valentin, C. E. Pollard, *J. Pharmacol. Toxicol. Methods* **2006**, *54*, 189 – 199.

[31] F. Persson, L. Carlsson, G. Duker, I. Jacobson, *J. Cardiovasc. Electrophysiol.* **2005**, *16*, 329 – 341.

[32] L. Jacobson, B. Middleton, J. Holmgren, S. Eirefelt, M. Fröjd, A. Blomgren, L. Gustavsson, *Assay Drug Dev. Technol.* **2007**, *5*, 403 – 415.

[33] C. L. Crespi, V. P. Miller, B. W. Penman, *Anal. Biochem.* **1997**, *248*, 188 – 190.

Received: January 28, 2015
Published online on March 20, 2015